Cooperative effects in spherical spasers

Ab initio analytical model

Bordo, Vladimir

Published in:
Physical Review B

DOI:
10.1103/PhysRevB.95.235412

Publication date:
2017

Document version
Publisher's PDF, also known as Version of record

Document license
CC BY-NC

Citation for pulished version (APA):
Bordo, V. (2017). Cooperative effects in spherical spasers: Ab initio analytical model. Physical Review B, 95(23), [235412]. https://doi.org/10.1103/PhysRevB.95.235412

Cooperative effects in spherical spasers: *Ab initio* analytical model

V. G. Bordo*

NanoSyd, Mads Clausen Institute, Syddansk Universitet, Alsion 2, DK-6400 Sønderborg, Denmark

(Received 13 March 2017; published 8 June 2017)

A fully analytical semiclassical theory of cooperative optical processes which occur in an ensemble of molecules embedded in a spherical core-shell nanoparticle is developed from first principles. Both the plasmonic Dicke effect and spaser generation are investigated for the designs in which a shell/core contains an arbitrarily large number of active molecules in the vicinity of a metallic core/shell. An essential aspect of the theory is an *ab initio* account of the feedback from the core/shell boundaries which significantly modifies the molecular dynamics. The theory provides rigorous, albeit simple and physically transparent, criteria for both plasmonic superradiance and surface plasmon generation.

DOI: 10.1103/PhysRevB.95.235412

I. INTRODUCTION

Recent progress in nanotechnology has led to the possibility to manipulate optical fields at the nanoscale. Strongly localized electromagnetic oscillations can be excited at metal surfaces and metal-dielectric interfaces, thus allowing shaping them by fabricating appropriate metallic nanostructures [1,2]. Such excitations, known as surface plasmon polaritons (SPPs), concentrate the power of the incident radiation into a small volume, thus providing an electromagnetic field intensity enhancement. This feature has been exploited in plenty of diverse applications in ultrasensitive sensing [3], subwavelength imaging [4], and ultrahigh-energy concentration [5], among other things.

A metal nanostructure can serve as an electromagnetic cavity which selects and amplifies certain electromagnetic modes. If such a cavity contains an optically active medium (i.e., a medium with population inversion), one can realize a nanoscale counterpart of the laser. This principle has received the name "surface plasmon amplification by stimulated emission of radiation" (spaser) [6]. The resonator of a spaser can be a metal nanoparticle whose size is much less than the wavelength of the generated electromagnetic field [7]. The active (gain) medium may be represented by semiconductor nanocrystals, dye molecules, rare-earth ions, or electron-hole excitations of a bulk semiconductor [7]. If at least one of the dimensions of the resonator is significantly longer than the wavelength, it is called a plasmon (or plasmonic) laser [8]. Such a device is outside the scope of our discussion.

Up to now, there has been only one claim of spaser experimental demonstration realized in gold nanoparticles (NPs) covered by silica shells which contained a large number ($\sim 2.7 \times 10^3$) of dye molecules [9]. The authors supported their observations with the model in which the gain is introduced as a negative contribution to the imaginary part of the refractive index of the silica shell. This approach implicitly assumes, however, that the polarization of the active molecules is determined by a predefined local electromagnetic field and the back action of the shell boundaries on the molecules can be neglected.

This experiment stimulated significant interest in theoretical modeling of core-shell spasers, both analytical [10–19] and numerical [23,24]. The analytical approach suggests different models which take into account the multiple-level structure of the active molecules, their saturation, the nonlocal optical response of the metallic core, and the retardation effect. Despite their diversity, all such models exploit the same unjustified simplification concerning the local field which was used in the original paper [9]. It is worthwhile to note, however, that the analysis carried out in Ref. [15] led to the conclusion that the results of Ref. [9] are more likely related to random lasing in a group of nanoparticles, rather than to spasing in single nanoparticles.

Careful modeling is critical to substantiating spaser claims [20] that demand a first-principles theory of the spaser operation. The dynamics of a nanoscale laser requires, in particular, consideration of the cavity-quantum-electrodynamical effects [21]. Besides the Purcell effect which expresses the modification of the relaxation rate in a cavity [22], one has to take into account the back-action of the electromagnetic field reflected from the cavity walls. These effects emerge naturally if one finds the polarization of the active molecules self-consistently assuming that the local field depends on the polarization itself.

The numerical approaches [23,24] have in their foundation such rigorous equations of the metal-core-active-shell dynamics. However, to reduce the computational challenges one is forced to implement the numerical calculations either for simplified structures or for simplified boundary conditions. In particular, the spaser operation was simulated for 1000 dye molecules oriented perpendicular to the NP surface [23], which does not reproduce the experimental conditions [9]. In Ref. [24] the boundary conditions for the electromagnetic field were imposed for a passive cavity which does not contain active molecules. In such an approach the feedback for the polarization of molecules provided by the reflective boundaries is missing. The authors obtained, however, a discrepancy with the experimental observations [9] in the threshold condition.

Besides the semiclassical theories discussed above one should mention also fully quantum numerical calculations [25–27]. These works investigate spaser generation in terms of the quantum correlation functions. Based on a numerically exact solution, the authors of Ref. [26] concluded that the claims of the spaser realization in Ref. [9] are probably

*bordo@mci.sdu.dk

incorrect. However, their calculations were implemented for a maximum of 30 quantum emitters, which is much smaller than the number utilized in the experiment.

Another aspect which is closely related to the spaser operation and is inherent in the spaser structure is the subwavelength confinement of the ensemble of active molecules. Such an ensemble emits coherent radiation cooperatively as a whole, which is referred to as the Dicke effect or superradiance [28–31]. The corresponding emission rate scales with the number of molecules. A similar effect takes place for a molecular ensemble located near a metal nanoparticle where the coupling between molecules is mediated by SPPs excited at the NP surface (the plasmonic Dicke effect or plasmon-mediated superradiance) [32,33]. This problem being formulated in the first-principles approach faces the same computational challenges as those mentioned above. Namely, the numerical calculations were implemented for a maximum of 100 emitter dipoles oriented perpendicular to the NP surface. One should also mention in this context a study [34] in which the superradiance of a large number of atoms near a metal NP is considered. The model exploited by the authors assumes, however, that all emitters are located on the surface of the NP shell.

Summarizing the above discussion, one can conclude that an approach to the spaser dynamics which, on the one hand, is developed from first principles and, on the other hand, is numerically feasible for a very large number of emitters for a wide range of parameters matching the experimental conditions is lacking in the literature. As a result, up to now a rigorous and clear answer to the question of whether the spasing conditions could be realized in the experiment (Ref. [9]) could not be given.

In the present paper, we bridge this gap in the semiclassical theory of spherical core-shell spasers. For this purpose, we exploit the approach developed by Prasad and Glauber [30,31] for the description of coherent radiation from a resonant medium which works especially well when the number density of active molecules is large. Namely, we replace the discrete structure of the medium by a continuous distribution of polarization, which is referred to as *polarium*.

This paper is organized as follows. In Sec. II we develop the theoretical formalism. First, we derive the electric field created by a single dipole in a core-shell structure and use this result to obtain the expression for the local field in the polarium. Then we write down the optical Bloch equations for the polarium. In Secs. III and IV we exploit them to investigate the plasmonic Dicke effect and the spaser operation, respectively, for one of the spaser designs. In Sec. V we introduce the modifications which correspond to the other spaser design. Section VI contains some numerical results and a brief discussion. In Sec. VII we formulate the main conclusions of the paper.

II. THEORETICAL FORMALISM

We consider an ensemble of N identical molecules in the vicinity of a metal surface interacting with the electromagnetic field and assume that the field frequency ω is close to the molecule transition frequency ω_0. The phenomenon discussed below has a rather general character; however, to be specific we consider two geometries of the system suggested in the literature [7,35], one of which matches the experimentally realized configuration [9].

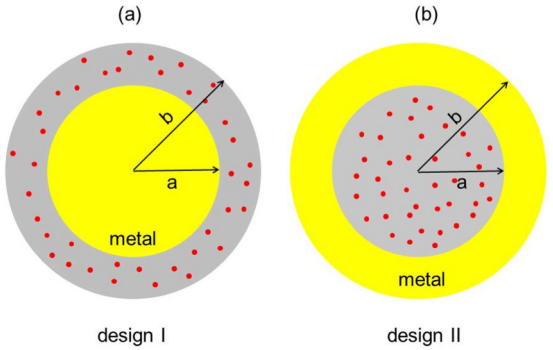

FIG. 1. Different designs of a core-shell spaser. (a) A metal core is surrounded by a dielectric shell doped with active molecules shown by red circles (design I). (b) A dielectric core doped with active molecules is surrounded by a metal shell (design II).

Namely, in the first design [design I; see Fig. 1(a)] we assume that a metal sphere of radius a is surrounded by a dielectric spherical shell of the outer radius b, which contains randomly oriented and randomly distributed molecules and which in turn is embedded in an infinite dielectric medium. The dielectric permittivities of the three media are $\epsilon_1(\omega)$, ϵ_2, and ϵ_3, respectively. In the second design [design II; see Fig. 1(b)] we assume that a dielectric sphere of radius a is doped by active molecules and is surrounded by a metallic shell of the outer radius b embedded in an infinite dielectric medium. The dielectric permittivities of the three media are ϵ_1, $\epsilon_2(\omega)$, and ϵ_3, respectively.

Restricting ourselves to the case where $a,b \ll \lambda = 2\pi c/\omega_0$, with c being the speed of light in vacuum, we describe the electromagnetic fields in the framework of the quasistatic approximation, i.e., in terms of an electrostatic potential ϕ which obeys the Laplace equation. In this limit SPP excitations are reduced to surface plasmons which represent collective oscillations of conduction electrons localized near a metal surface. First, we derive the theory for design I, and then we consider the modifications which should be introduced for design II.

A. Dipole field

As a preliminary problem we consider the electrostatic potential in the system with a single molecular dipole $\mathbf{p}$ located at point $\mathbf{x}'$ with spherical coordinates r', θ', and φ'. The potential at the observation point $\mathbf{x} = (r,\theta,\varphi)$ can be expanded in terms of the spherical harmonics $Y_{lm}(\theta,\varphi)$ as follows [36]:

$$\phi^{(1)}(\mathbf{x}) = \sum_{lm} a_{lm}^{(1)} r^l Y_{lm}(\theta,\varphi), \tag{1}$$

$$\phi^{(2)}(\mathbf{x}) = \frac{1}{\epsilon_2}\sum_{lm}\frac{1}{2l+1}\mathbf{p}\cdot\nabla'\left[\frac{r_<^l}{r_>^{l+1}}Y_{lm}^*(\theta',\varphi')\right]Y_{lm}(\theta,\varphi) + \sum_{lm} a_{lm}^{(2)} r^l Y_{lm}(\theta,\varphi) + \sum_{lm} b_{lm}^{(2)}\frac{1}{r^{l+1}}Y_{lm}(\theta,\varphi), \tag{2}$$

$$\phi^{(3)}(\mathbf{x}) = \sum_{lm} b_{lm}^{(3)}\frac{1}{r^{l+1}}Y_{lm}(\theta,\varphi). \tag{3}$$

Here the potentials $\phi^{(i)}$ refer to the regions with the dielectric permittivity ϵ_i, $r_< = \min(r,r')$, $r_> = \max(r,r')$, and the prime above the nabla operator implies that it acts on the primed variables. The coefficients $a_{lm}^{(i)}$ and $b_{lm}^{(i)}$ depend on the position of the dipole $\mathbf{x}'$ and are determined from the boundary conditions

$$\phi^{(1)}(r=a) = \phi^{(2)}(r=a), \tag{4}$$

$$\epsilon_1\left(\frac{\partial\phi^{(1)}}{\partial r}\right)_{r=a} = \epsilon_2\left(\frac{\partial\phi^{(2)}}{\partial r}\right)_{r=a}, \tag{5}$$

$$\phi^{(2)}(r=b) = \phi^{(3)}(r=b), \tag{6}$$

$$\epsilon_2\left(\frac{\partial\phi^{(2)}}{\partial r}\right)_{r=b} = \epsilon_3\left(\frac{\partial\phi^{(3)}}{\partial r}\right)_{r=b}. \tag{7}$$

In particular, coefficients $a_{lm}^{(2)}$ and $b_{lm}^{(2)}$ are found as

$$a_{lm}^{(2)}(\mathbf{x}') = \mathbf{p}\cdot\mathbf{F}_{lm}(\mathbf{x}'), \tag{8}$$

$$b_{lm}^{(2)}(\mathbf{x}') = \mathbf{p}\cdot\mathbf{G}_{lm}(\mathbf{x}'), \tag{9}$$

where

$$\mathbf{F}_{lm}(\mathbf{x}) \equiv \alpha_{1l}\mathbf{g}_{lm}^{*}(\mathbf{x}) + \alpha_{2l}\mathbf{f}_{lm}^{*}(\mathbf{x}), \tag{10}$$

$$\mathbf{G}_{lm}(\mathbf{x}) \equiv \beta_{1l}\mathbf{g}_{lm}^{*}(\mathbf{x}) + \beta_{2l}\mathbf{f}_{lm}^{*}(\mathbf{x}), \tag{11}$$

with

$$\mathbf{f}_{lm}(\mathbf{x}) \equiv \nabla[r^l Y_{lm}(\theta,\varphi)], \tag{12}$$

$$\mathbf{g}_{lm}(\mathbf{x}) \equiv \nabla\left[\frac{Y_{lm}(\theta,\varphi)}{r^{l+1}}\right], \tag{13}$$

and the constants α_{1l}, α_{2l}, β_{1l}, and β_{2l} are given in Appendix A. The first term on the right-hand side of Eq. (2) is the potential of the point dipole $\mathbf{p}$ in an unbounded medium, whereas the other two terms represent the influence of the spherical layer boundaries.

B. Polarium model

Let us turn now to the case where N identical molecules are uniformly distributed within the spherical shell volume V. We follow the approach by Prasad and Glauber [30,31], who described such an ensemble as a continuous medium (polarium) characterized by its polarization $\mathbf{P}(\mathbf{x})$. Then the electric field amplitude in the spherical shell interior, which originates from the molecular dipoles, is found as

$$\begin{aligned}\mathbf{E}^{(2)}(\mathbf{x}) &= -\nabla\int_V \phi^{(2)}(\mathbf{x},\mathbf{x}')d\mathbf{x}' \\ &= \mathbf{E}_P(\mathbf{x}) - \sum_{lm}\mathbf{f}_{lm}(\mathbf{x})\int_V \mathbf{P}(\mathbf{x}')\cdot\mathbf{F}_{lm}(\mathbf{x}')d\mathbf{x}' \\ &\quad - \sum_{lm}\mathbf{g}_{lm}(\mathbf{x})\int_V \mathbf{P}(\mathbf{x}')\cdot\mathbf{G}_{lm}(\mathbf{x}')d\mathbf{x}'.\end{aligned} \tag{14}$$

The field $\mathbf{E}_P$ in Eq. (14) originates from the molecular dipole potentials which stem from the first term on the right-hand side of Eq. (2). Assuming that the number of molecules N is large, it can be found, to a good approximation, as the polarization contribution to the Lorentz local field, i.e., in Gaussian units [37]

$$\mathbf{E}_P(\mathbf{x}) = \frac{4\pi}{3\epsilon_2}\mathbf{P}(\mathbf{x}), \tag{15}$$

where we have taken into account the dielectric permittivity of the host material.

Then the local field in the shell can be represented as

$$\mathbf{E} = \mathbf{E}_0 + \mathbf{E}^{(2)} = \mathbf{E}_0 + \mathbf{E}_P + \mathbf{E}_s = \mathbf{E}_L + \mathbf{E}_s, \tag{16}$$

where $\mathbf{E}_0$ is the average macroscopic field in the polarium, $\mathbf{E}_s$ is the contribution of the last two terms on the right-hand side of Eq. (14), which describe the influence of the spherical shell surfaces, and $\mathbf{E}_L$ is the well-known Lorentz local field [37].

The local field, Eq. (16), contains contributions from all multipole modes specified by the integers $\{lm\}$, which are determined by the coefficients α_{1l}, α_{2l}, β_{1l}, and β_{2l}, Eq. (A1). These coefficients have resonances when their common denominator

$$\begin{aligned}D_l(\omega) \equiv{}& [l\epsilon_1(\omega) + (l+1)\epsilon_2][l\epsilon_2 + (l+1)\epsilon_3] \\ &+ l(l+1)[\epsilon_2 - \epsilon_1(\omega)](\epsilon_3 - \epsilon_2)\left(\frac{a}{b}\right)^{2l+1}\end{aligned} \tag{17}$$

is close to zero. In what follows, we consider the case where the molecular transition frequency ω_0 falls into the frequency band of the dipole surface plasmon mode ($l = 1$) which gives the dominant contribution to the field.

C. Optical Bloch equations

We shall model the molecules in the polarium by two-level systems with the ground state $|1\rangle$, excited state $|2\rangle$, transition frequency ω_0, and transition dipole moment μ_{12}. We assume that the transition $|2\rangle \rightarrow |1\rangle$ is characterized by the transverse relaxation rate $\gamma_\perp$, which is dominated by the nonradiative phase relaxation and determines the transition homogeneous linewidth, and the transition dipole moments of molecules are randomly oriented. Let us note that the models adopted in Refs. [30–33] imply that $\gamma_\perp \equiv 0$.

Let us assume now that the system is excited by an electromagnetic field of frequency ω which is close to ω_0. It can be decomposed into the negative and positive frequency parts as

$$\mathbf{E}(t) = \mathbf{E}^{(-)}(t)e^{i\omega t} + \mathbf{E}^{(+)}(t)e^{-i\omega t}, \tag{18}$$

$$\mathbf{E}^{(-)}(t) = [\mathbf{E}^{(+)}(t)]^*, \tag{19}$$

where the amplitudes $\mathbf{E}^{(\pm)}(t)$ vary in time much slower than $\exp(\pm i\omega t)$. The polarium polarization has a similar form,

$$\mathbf{P}(t) = \mathbf{P}^{(-)}(t)e^{i\omega t} + \mathbf{P}^{(+)}(t)e^{-i\omega t}, \tag{20}$$

$$\mathbf{P}^{(-)}(t) = [\mathbf{P}^{(+)}(t)]^*, \tag{21}$$

where the negative and positive frequency parts satisfy the optical Bloch equations [38]

$$\begin{aligned}\frac{\partial\mathbf{P}^{(+)}(t)}{\partial t} &= -(\gamma_\perp - i\Delta)\mathbf{P}^{(+)}(t) \\ &\quad - \frac{i}{3\hbar}|\mu_{12}|^2 D(t)\mathbf{E}^{(+)}(t),\end{aligned} \tag{22}$$

$$\frac{\partial D(t)}{\partial t} = -\gamma_{\parallel}[D(t) - D_0] + \frac{2i}{\hbar}[\mathbf{P}^{(-)}(t)\mathbf{E}^{(+)}(t) - \mathbf{P}^{(+)}(t)\mathbf{E}^{(-)}(t)]. \quad (23)$$

Here $\Delta = \omega - \omega_0$ is the resonance detuning, $\gamma_{\parallel}$ is the longitudinal relaxation rate of the transition $|2\rangle \to |1\rangle$ which takes into account the Purcell effect [22], $D = \rho(n_2 - n_1)$, with $\rho = N/V$ being the number density of molecules and n_1 and n_2 being the populations of the ground and excited states, respectively, and D_0 is the equilibrium value of D. The factor $1/3$ in front of $|\mu_{12}|^2$ in Eq. (22) originates from averaging over the orientations of molecules.

In the case of a weak electromagnetic field the population difference density D does not differ significantly from its equilibrium value, and Eq. (22) is uncoupled from Eq. (23), taking the form

$$\frac{\partial \mathbf{P}^{(+)}(t)}{\partial t} + (\gamma_{\perp} - i\Delta)\mathbf{P}^{(+)}(t) = -\frac{i}{3\hbar}|\mu_{12}|^2 D_0 \mathbf{E}^{(+)}(t). \quad (24)$$

III. PLASMONIC DICKE EFFECT

Let us consider the system in the absence of the external macroscopic field ($\mathbf{E}_0 = 0$) and assume that there is some initial polarization of the polarium created, for example, by a short laser pulse. Then the evolution of the system is described by the equation

$$\frac{\partial \mathbf{P}^{(+)}(t)}{\partial t} + (\gamma_{\perp} - i\Delta')\mathbf{P}^{(+)}(t) = \frac{i}{3\hbar}\rho|\mu_{12}|^2 \mathbf{E}_s^{(+)}(t), \quad (25)$$

with the initial condition $\mathbf{P}^{(+)}(0) = \mathbf{P}_0^{(+)}$, where we have assumed that the population of the excited state is negligible. Here we have taken into account that the local field oscillates at the frequency of the molecular transition ω_0. We have also moved the term proportional to $\mathbf{E}_P$ to the left-hand side and introduced the renormalized transition frequency [30]

$$\omega_0' = \omega_0 - \frac{4\pi}{9\hbar\epsilon_2}\rho|\mu_{12}|^2 \quad (26)$$

and renormalized resonance detuning

$$\Delta' = \omega_0 - \omega_0' = \frac{4\pi}{9\hbar\epsilon_2}\rho|\mu_{12}|^2. \quad (27)$$

Equation (25) can be analyzed by applying the Laplace transform

$$\tilde{\mathbf{P}}^{(+)}(\mathbf{x},s) = \int_0^{\infty} \mathbf{P}^{(+)}(\mathbf{x},t)e^{-st}dt, \quad (28)$$

with $s = \sigma + i\Omega$ being the complex variable. It is then reduced to the integral equation

$$\tilde{\mathbf{P}}^{(+)}(\mathbf{x},s) + \chi'(s)\int_V \bar{K}(\mathbf{x},\mathbf{x}')\tilde{\mathbf{P}}^{(+)}(\mathbf{x}',s)d\mathbf{x}' = \frac{\mathbf{P}_0^{(+)}(\mathbf{x})}{s + \gamma_{\perp} - i\Delta'}, \quad (29)$$

where the kernel dyadic $\bar{K}(\mathbf{x},\mathbf{x}')$ has a degenerate form [39],

$$\bar{K}(\mathbf{x},\mathbf{x}') = \mathbf{f}_{10}(\mathbf{x})\mathbf{F}_{10}(\mathbf{x}') + \mathbf{g}_{10}(\mathbf{x})\mathbf{G}_{10}(\mathbf{x}') \quad (30)$$

and

$$\chi'(s) = \frac{i\kappa}{s + \gamma_{\perp} - i\Delta'}, \quad (31)$$

where

$$\kappa = \frac{1}{3\hbar}\rho|\mu_{12}|^2 \quad (32)$$

is the Laplace transform of the linear susceptibility of the polarium. We have assumed here that the initial polarization is created by a spatially uniform field linearly polarized along the z axis so that a nonzero contribution originates only from $m = 0$.

Taking a scalar product of Eq. (29) from the left with either $\mathbf{F}_{10}(\mathbf{x})$ or $\mathbf{G}_{10}(\mathbf{x})$ and integrating it over the volume V, one obtains two linear algebraic equations, which can be compactly written in the vector form

$$\vec{\mathcal{P}}(s) + \chi'(s)\hat{M}\vec{\mathcal{P}}(s) = \frac{\vec{\mathcal{P}}_0}{s + \gamma_{\perp} - i\Delta'}, \quad (33)$$

where the components of the vectors $\vec{\mathcal{P}}$ and $\vec{\mathcal{P}}_0$ are given by

$$\mathcal{P}_1(s) = \int_V \mathbf{F}_{10}(\mathbf{x}) \cdot \tilde{\mathbf{P}}^{(+)}(\mathbf{x},s)d\mathbf{x}, \quad (34)$$

$$\mathcal{P}_2(s) = \int_V \mathbf{G}_{10}(\mathbf{x}) \cdot \tilde{\mathbf{P}}^{(+)}(\mathbf{x},s)d\mathbf{x}, \quad (35)$$

$$\mathcal{P}_{0,1} = \int_V \mathbf{F}_{10}(\mathbf{x}) \cdot \mathbf{P}_0^{(+)}(\mathbf{x})d\mathbf{x}, \quad (36)$$

$$\mathcal{P}_{0,2} = \int_V \mathbf{G}_{10}(\mathbf{x}) \cdot \mathbf{P}_0^{(+)}(\mathbf{x})d\mathbf{x} \quad (37)$$

and the matrix elements of the matrix $\hat{M}$ are given by

$$M_{11} = \int_V \mathbf{F}_{10}(\mathbf{x}) \cdot \mathbf{f}_{10}(\mathbf{x})d\mathbf{x}, \quad (38)$$

$$M_{12} = \int_V \mathbf{F}_{10}(\mathbf{x}) \cdot \mathbf{g}_{10}(\mathbf{x})d\mathbf{x}, \quad (39)$$

$$M_{21} = \int_V \mathbf{G}_{10}(\mathbf{x}) \cdot \mathbf{f}_{10}(\mathbf{x})d\mathbf{x}, \quad (40)$$

$$M_{22} = \int_V \mathbf{G}_{10}(\mathbf{x}) \cdot \mathbf{g}_{10}(\mathbf{x})d\mathbf{x}. \quad (41)$$

The solution of Eq. (33) is found as

$$\vec{\mathcal{P}}(s) = \frac{1}{i\kappa}[\hat{M} - \lambda'(s)\hat{I}]^{-1}\vec{\mathcal{P}}_0, \quad (42)$$

with

$$\lambda'(s) = -\frac{1}{\chi'(s)} \quad (43)$$

and $\hat{I}$ being a unit 2×2 matrix, or, in an explicit form,

$$\begin{pmatrix} \mathcal{P}_1(s) \\ \mathcal{P}_2(s) \end{pmatrix} = \frac{1}{i\kappa D'(s)} \begin{pmatrix} M_{22} - \lambda'(s) & -M_{12} \\ -M_{21} & M_{11} - \lambda'(s) \end{pmatrix} \begin{pmatrix} \mathcal{P}_{0,1} \\ \mathcal{P}_{0,2} \end{pmatrix}, \quad (44)$$

with

$$D'(s) = [\lambda'(s) - \lambda_1][\lambda'(s) - \lambda_2] \quad (45)$$

being the determinant of the matrix $\hat{M} - \lambda'(s)\hat{I}$ and $\lambda_j = \lambda_j' + i\lambda_j''$ $(j = 1,2)$ being the eigenvalues of the matrix $\hat{M}$.

Finally, the solution of Eq. (29) can be expressed in terms of $\mathcal{P}_1(s)$ and $\mathcal{P}_2(s)$ as follows:

$$\tilde{\mathbf{P}}^{(+)}(\mathbf{x},s) = \frac{\mathbf{P}_0^{(+)}(\mathbf{x})}{s+\gamma_\perp - i\Delta'} - \chi'(s)[\mathcal{P}_1(s)\mathbf{f}_{10}(\mathbf{x}) + \mathcal{P}_2(s)\mathbf{g}_{10}(\mathbf{x})]. \quad (46)$$

The function $\tilde{\mathbf{P}}^{(+)}(s)$, Eq. (46), has three poles:

$$s_0 = -\gamma_\perp + i\Delta', \quad (47)$$

$$s_1 = -\gamma_\perp - i\kappa\lambda_1 + i\Delta', \quad (48)$$

$$s_2 = -\gamma_\perp - i\kappa\lambda_2 + i\Delta'. \quad (49)$$

Let us note that the quantities $\kappa\lambda_j \sim \rho(b^3 - a^3) \sim N$; that is, they represent a cooperative effect of all N molecules. These terms describe an N-fold enhancement of the relaxation rate due to the plasmonic Dicke effect [32,33] provided that $\lambda_j'' < 0$. This effect is essential only if $\kappa|\lambda_j''| \geqslant \gamma_\perp$. Otherwise, the coherence between the molecules decays faster than their cooperative emission is established. In the limit $\gamma_\perp \to 0$ the mode associated with the pole s_0 can be identified as a subradiant mode [32,33], while the character of the other two modes depends on the magnitude of $\kappa\lambda_j''$.

The time evolution of the positive frequency part of the polarium polarization is found as

$$\mathbf{P}^{(+)}(\mathbf{x},t) = \mathbf{P}_0^{(+)}(\mathbf{x})e^{s_0 t} + \sum_{j=0}^{2} \mathbf{Q}_j(\mathbf{x})e^{s_j t}, \quad (50)$$

with

$$\mathbf{Q}_j(\mathbf{x}) = -\sigma_j\{[(M_{22} - \lambda_j)\mathcal{P}_{0,1} - M_{12}\mathcal{P}_{0,2}]\mathbf{f}_{10}(\mathbf{x}) + [-M_{21}\mathcal{P}_{0,1} + (M_{11} - \lambda_j)\mathcal{P}_{0,2}]\mathbf{g}_{10}(\mathbf{x})\}, \quad (51)$$

where

$$\sigma_0 = \frac{1}{\lambda_1\lambda_2}, \quad (52)$$

$$\sigma_1 = \frac{1}{\lambda_1(\lambda_1 - \lambda_2)}, \quad (53)$$

$$\sigma_2 = \frac{1}{\lambda_2(\lambda_2 - \lambda_1)}, \quad (54)$$

and $\lambda_0 = \lambda'(s_0) = 0$.

The polarization (50) determines the evolution of the local electromagnetic field, Eq. (16). Its positive frequency part, which originates from the spherical layer boundaries, is found explicitly as follows:

$$\mathbf{E}_s^{(+)}(\mathbf{x},t) = \sqrt{\frac{4\pi}{3}}\frac{P_0^{(+)}}{\lambda_2 - \lambda_1} \times \{-\lambda_1[(\lambda_2 - M_{11})\mathbf{f}_{10}(\mathbf{x}) - M_{21}\mathbf{g}_{10}(\mathbf{x})]e^{s_1 t} + \lambda_2[(\lambda_1 - M_{11})\mathbf{f}_{10}(\mathbf{x}) - M_{21}\mathbf{g}_{10}(\mathbf{x})]e^{s_2 t}\}, \quad (55)$$

where we have assumed that the initial polarization is uniform and is directed along the z axis: $\mathbf{P}_0^{(+)}(\mathbf{x}) = P_0^{(+)}\mathbf{e}_z$, with $\mathbf{e}_z$ being a unit vector along the z axis. The initial value of this field can be written in the form

$$\mathbf{E}_s^{(+)}(\mathbf{x},0) = -\sqrt{\frac{3}{4\pi}}P_0^{(+)}V[\alpha_{21}(\omega_0)\mathbf{f}_{10}(\mathbf{x}) + \beta_{21}(\omega_0)\mathbf{g}_{10}(\mathbf{x})], \quad (56)$$

where $V = (4\pi/3)(b^3 - a^3)$ is the volume of the spherical layer. Its amplitude is proportional to the initial dipole moment of the polarium $P_0^{(+)}V$ and hence to the total number of molecules N. Accordingly, the intensity of the local field scales as N^2, which signifies a coherent local-field enhancement.

IV. SPASER GENERATION

The structure under consideration can generate electromagnetic field when a population inversion is created in the active molecules by an external optical pumping. To determine the criterion for the field generation in the system, we follow an approach which is conventional in laser theory [38,40]. Namely, we assume that, initially, there is no local field at the frequency ω_0 ($\mathbf{E} = 0$), and we investigate the conditions under which the system is unstable with respect to a small increment in the average macroscopic field $\delta\mathbf{E}_0$.

Taking a uniform field linearly polarized along the z axis, one can write the dominant (dipole) contribution to the positive-frequency part of the local field as follows:

$$\delta\mathbf{E}^{(+)}(\mathbf{x},t) = \delta\mathbf{E}_0^{(+)} + \mathbf{E}_P^{(+)}(\mathbf{x},t) - \int_V \bar{K}(\mathbf{x},\mathbf{x}')\mathbf{P}^{(+)}(\mathbf{x}',t)d\mathbf{x}', \quad (57)$$

where the kernel $\bar{K}(\mathbf{x},\mathbf{x}')$ is given by Eq. (30) and we have taken into account the axial symmetry of the problem. The polarization $\mathbf{P}^{(+)}(\mathbf{x},t)$ satisfies in its turn Eq. (24), in which the right-hand side contains $\delta\mathbf{E}^{(+)}(\mathbf{x},t)$ and the equilibrium value of the population inversion density D_0 is determined by the optical pumping.

Taking the Laplace transform of both Eqs. (57) and (24), one comes to the integral equation for the Laplace-transformed quantity $\delta\tilde{\mathbf{E}}^{(+)}(\mathbf{x},s)$,

$$\left[1 + \frac{4\pi}{3\epsilon_2}w_0\chi_0(s)\right]\delta\tilde{\mathbf{E}}^{(+)}(\mathbf{x},s) - w_0\chi_0(s)\int_V \bar{K}(\mathbf{x},\mathbf{x}')\delta\tilde{\mathbf{E}}^{(+)}(\mathbf{x}',s)d\mathbf{x}' = \frac{\delta\mathbf{E}_0^{(+)}}{s}, \quad (58)$$

where $w_0 = n_2^0 - n_1^0$ is the equilibrium value of the population difference and

$$\chi_0(s) = \frac{i\kappa}{s + \gamma_\perp}. \quad (59)$$

Equation (58) is reduced to the vector equation

$$\delta\vec{\mathcal{E}}(s) + \mu(s)\hat{M}\delta\vec{\mathcal{E}}(s) = \frac{(s+\gamma_\perp)\delta\vec{\mathcal{E}}_0}{s(s + \gamma_\perp - i\tilde{\Delta})}, \quad (60)$$

where

$$\delta\mathcal{E}_1(s) = \int_V \mathbf{F}_{10}(\mathbf{x}) \cdot \delta\tilde{\mathbf{E}}^{(+)}(\mathbf{x},s)d\mathbf{x}, \quad (61)$$

$$\delta\mathcal{E}_2(s) = \int_V \mathbf{G}_{10}(\mathbf{x}) \cdot \delta\tilde{\mathbf{E}}^{(+)}(\mathbf{x},s)d\mathbf{x}, \quad (62)$$

$$\delta\mathcal{E}_{0,1} = \int_V \mathbf{F}_{10}(\mathbf{x}) \cdot \delta\mathbf{E}_0^{(+)}d\mathbf{x}, \quad (63)$$

$$\delta\mathcal{E}_{0,2} = \int_V \mathbf{G}_{10}(\mathbf{x}) \cdot \delta\mathbf{E}_0^{(+)} d\mathbf{x}, \tag{64}$$

$$\mu(s) = -\frac{w_0\chi_0(s)}{1 + (4\pi/3\epsilon_2)w_0\chi_0(s)}, \tag{65}$$

and

$$\tilde{\Delta} = -\frac{4\pi}{9\hbar\epsilon_2} D_0|\mu_{12}|^2 \tag{66}$$

is the renormalized frequency detuning.

Similar to Eq. (33), the evolution of the solution of Eq. (60) is determined by, besides the poles $s = 0$ and $s = -\gamma_\perp + i\tilde{\Delta}$, the zeros of the determinant of the matrix $\hat{M} - \lambda(s)\hat{I}$ with

$$\lambda(s) = -\frac{1}{\mu(s)}. \tag{67}$$

These zeros can be explicitly written as ($j = 1,2$)

$$\tilde{s}_j = -\gamma_\perp + i w_0\kappa\lambda_j + i\tilde{\Delta}, \tag{68}$$

where $\lambda_j = \lambda_j' + i\lambda_j''$ are the eigenvalues of the matrix $\hat{M}$.

The two poles given by Eq. (68) correspond to two modes of the local-field evolution $\mathbf{E}^{(+)}(t) \sim \exp(\tilde{s}_j t)$. Their imaginary parts specify the frequency-pulling effect for the mode frequency,

$$\omega_j = \omega_0 - \frac{1}{3\hbar} D_0|\mu_{12}|\left(\lambda_j' - \frac{4\pi}{3\epsilon_2}\right). \tag{69}$$

The evolution of the local-field amplitude is determined by the quantities $\mathrm{Re}(\tilde{s}_j) = -\gamma_\perp - w_0\kappa\lambda_j''$. If $\lambda_j'' < 0$ and $w_0 > 0$ (i.e., a population inversion takes place), the terms $-w_0\kappa\lambda_j''$ describe a cooperative amplification of the local field. If, besides that,

$$-w_0\kappa\lambda_j'' = -\frac{1}{3\hbar} D_0|\mu_{12}|^2\lambda_j'' > \gamma_\perp, \tag{70}$$

such a pole corresponds to an exponential increase in the local field with time, i.e., to the generation of the dipole surface plasmon mode. In such a case Eq. (70) represents a threshold condition for generation (spasing) imposed on the population inversion density D_0. A comparison of criterion (70) with Eqs. (48) and (49) reveals that spasing in the system is possible only if the plasmonic superradiance in such a system prevails over the phase relaxation.

Some important conclusions follow from the above analytical theory. (i) The eigenvalues λ_j, and hence the threshold condition (70), depend only on the ratio a/b, rather than on the absolute values of a and b. This property suggests a scaling law for the threshold criterion. (ii) If $a \ll b \ll \lambda$, then $\lambda_1'' \approx 0$ and $\lambda_2'' < 0$. In such a case only one mode can be spasing. (iii) If $a \sim b \ll \lambda$ and $\mathrm{Im}(\epsilon_1) \ll |\mathrm{Re}(\epsilon_1)|$, which takes place in the infrared spectral range, then $\lambda_{1,2}'' \approx 0$, and the spasing effect is impossible.

V. SPASER IN DESIGN II

In design II, the molecules are located within a spherical region. For a single molecular dipole $\mathbf{p}$ the potential at the observation point is expanded in terms of the spherical harmonics as follows:

$$\phi^{(1)}(\mathbf{x}) = \frac{1}{\epsilon_1}\sum_{lm}\frac{1}{2l+1}\mathbf{p}\cdot\nabla'\left[\frac{r_<^l}{r_>^{l+1}}Y_{lm}^*(\theta',\varphi')\right]Y_{lm}(\theta,\varphi) + \sum_{lm} a_{lm}^{(1)} r^l Y_{lm}(\theta,\varphi), \tag{71}$$

$$\phi^{(2)}(\mathbf{x}) = \sum_{lm} a_{lm}^{(2)} r^l Y_{lm}(\theta,\varphi) + \sum_{lm} b_{lm}^{(2)}\frac{1}{r^{l+1}}Y_{lm}(\theta,\varphi), \tag{72}$$

$$\phi^{(3)}(\mathbf{x}) = \sum_{lm} b_{lm}^{(3)}\frac{1}{r^{l+1}}Y_{lm}(\theta,\varphi), \tag{73}$$

where the coefficients $a_{lm}^{(i)}$ and $b_{lm}^{(i)}$ are determined from the boundary conditions (4)–(7). In particular, $a_{lm}^{(1)}$ is found as

$$a_{lm}^{(1)}(\mathbf{x}) = \delta_l \mathbf{p}\cdot\mathbf{f}_{lm}(\mathbf{x}), \tag{74}$$

where the coefficient δ_l is given in Appendix A.

Correspondingly, for an ensemble of dipoles distributed within the spherical core the electric field is found as

$$\mathbf{E}^{(1)}(\mathbf{x}) = -\nabla\int_V \phi^{(1)}(\mathbf{x},\mathbf{x}')d\mathbf{x}' = \mathbf{E}_P(\mathbf{x}) - \sum_{lm}\delta_l\mathbf{f}_{lm}(\mathbf{x})\int_V \mathbf{P}(\mathbf{x}')\cdot\mathbf{f}_{lm}^*(\mathbf{x}')d\mathbf{x}', \tag{75}$$

where $\mathbf{E}_P$ is defined by Eq. (15) with ϵ_2 being replaced by ϵ_1 and $V = (4/3)\pi a^3$ is the core volume.

When considering the plasmonic Dicke effect, one obtains an integral equation for the Laplace transform of the polarium polarization which formally coincides with Eq. (29) but in which the kernel is defined as

$$\bar{K}(\mathbf{x},\mathbf{x}') = \delta_1\mathbf{f}_{10}(\mathbf{x})\mathbf{f}_{10}(\mathbf{x}'). \tag{76}$$

Accordingly, instead of the vector equation (33), one comes to a scalar equation

$$[1 + \mathcal{M}\bar{\chi}(s)]\mathcal{P}(s) = \frac{\mathcal{P}_0}{s + \gamma_\perp - i\bar{\Delta}}, \tag{77}$$

with

$$\mathcal{P}(s) = \int_V \mathbf{f}_{10}(\mathbf{x})\cdot\tilde{\mathbf{P}}^{(+)}(\mathbf{x},s)d\mathbf{x}, \tag{78}$$

$$\mathcal{P}_0 = \int_V \mathbf{f}_{10}(\mathbf{x})\cdot\mathbf{P}_0^{(+)}(\mathbf{x})d\mathbf{x}, \tag{79}$$

and

$$\mathcal{M} = \delta_1\int_V |\mathbf{f}_{10}(\mathbf{x})|^2 d\mathbf{x} = \delta_1 a^3. \tag{80}$$

Let us note that the quantity $\mathcal{M}$ depends on the ratio a/b rather than on the absolute values of a and b.

The evolution of the polarization is determined by, besides the pole $s = -\gamma_\perp + i\bar{\Delta}$, the pole

$$s_3 = -\gamma_\perp - i\kappa\mathcal{M} + i\bar{\Delta}, \tag{81}$$

which provides a zero value for the left-hand side of Eq. (77). Here the term $-i\kappa\mathcal{M}$ is proportional to the number of

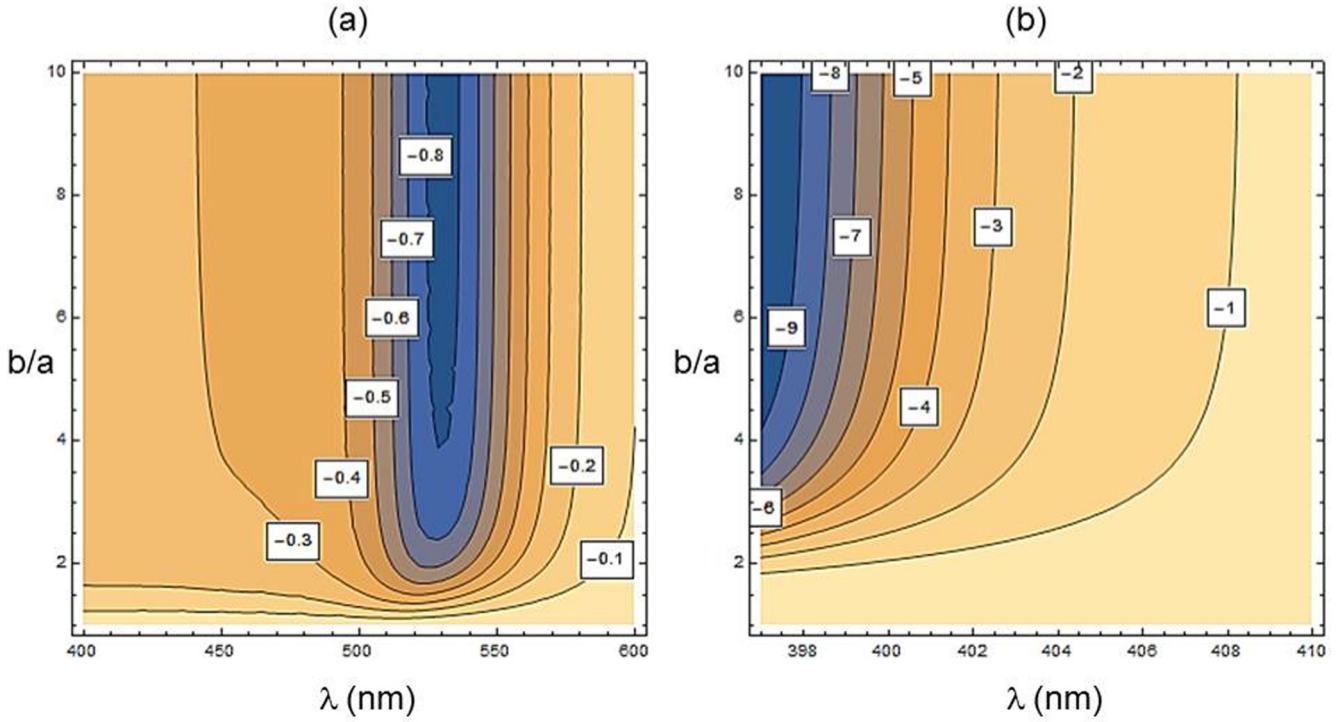

FIG. 2. Contour plots of λ_2'' in the vicinity of the resonance between the molecule transition ($\lambda = 2\pi c/\omega_0$) and the dipole surface plasmon mode ($l = 1$). (a) Gold core. (b) Silver core.

molecules N, and its real part describes the plasmonic Dicke effect in design II.

The local field inside the core is uniform and is directed along the z axis. The temporal evolution of its part related to the core-shell boundary corresponds to the plasmonic Dicke effect and is given by

$$\mathbf{E}_s^{(+)}(\mathbf{x},t) = -P_0^{(+)}a^3\delta_1(\omega_0)e^{s_3 t}\mathbf{e}_z. \tag{82}$$

Turning to the spaser generation in design II, one should replace the matrix $\hat{M}$ in Eq. (60) by the quantity $\mathcal{M}$. Correspondingly, the quantities λ' and λ'' in Eqs. (69) and (70) should be replaced by $\mathrm{Re}\mathcal{M}$ and $\mathrm{Im}\mathcal{M}$, respectively.

VI. NUMERICAL RESULTS AND DISCUSSION

A. Design I

We illustrate the above theory by the calculations beginning with the spaser parameters which correspond to the experiment (Ref. [9]). Taking $a = 7$ nm, $b = 22$ nm, and $N = 2.7 \times 10^3$, one obtains $\rho = 6.3 \times 10^{19}$ cm^{-3}. Assuming the same typical values of parameters for active molecules as in Ref. [23], $\hbar\gamma_\perp = 0.05$ eV ($\gamma_\perp = 1.2 \times 10^{13}$ s^{-1}) and $|\mu_{12}| = 4$ D, one finds $\kappa = 3.3 \times 10^{11}$ s^{-1} and $\kappa/\gamma_\perp = 2.8 \times 10^{-2}$.

Both the Dicke effect and the spaser dynamics in design I are determined by the eigenvalues of the matrix $\hat{M}$, λ_1 and λ_2, which depend on the wavelength of the local field λ and the ratio b/a. For one of them $|\lambda_1''| \sim 10^{-7}$–$10^{-6}$ in the considered range of parameters. This gives $\kappa|\lambda_1''|/\gamma_\perp \sim 10^{-9}$–$10^{-8}$ and $\kappa|\lambda_1''| \sim 10^4$–$10^5$ s^{-1}, and thus this mode can be identified as subradiant.

The contour plots of λ_2'' in the parameter plane $\lambda - b/a$ are shown in Fig. 2 for both Au and Ag cores. The corresponding mode is superradiant. In this case $\kappa|\lambda_2''|/\gamma_\perp \sim 10^{-3}$–$10^{-2}$ for the given parameters, which means that the cooperative emission is insignificant. The comparison of Figs. 2(a) and 2(b) reveals that the cooperative effect is more essential in a nanoparticle with a silver core. In the vicinity of the resonance with the dipole surface plasmon mode its contribution increases with the ratio b/a. The role of the cooperative emission can be enhanced if either a more heavily doped shell with $\rho \geqslant 10^{21}$ cm^{-3} is used or the nanoparticles are cooled down to a cryogenic temperature that considerably reduces $\gamma_\perp$ [41].

The same parameters determine the possibility of the dipole surface plasmon generation in a core-shell spaser. The minimal

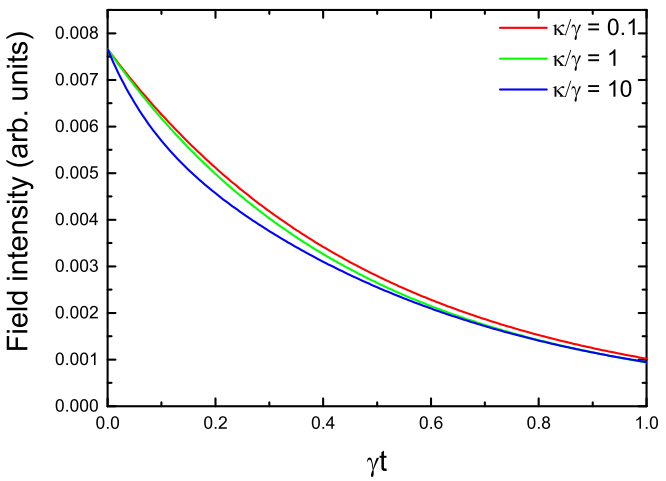

FIG. 3. The local-field intensity for a gold core at $r = b$ and $\theta = 0$ as a function of the dimensionless time $\gamma_\perp t$ for different ratios $\kappa/\gamma_\perp$. Here $\lambda = 525$ nm, $b/a = 3.14$.

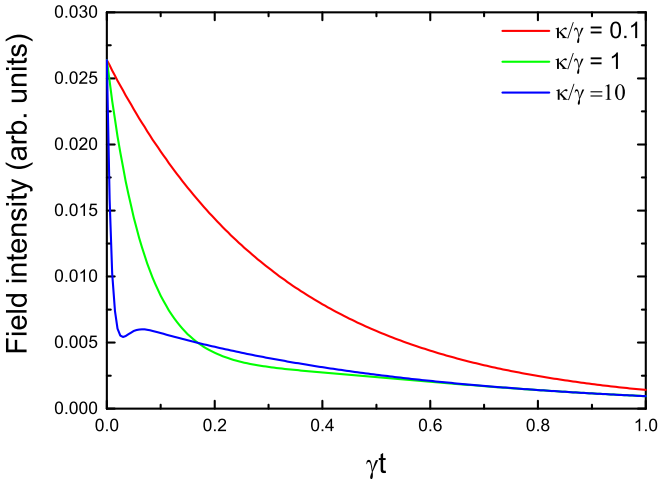

FIG. 4. The same as in Fig. 3, but for a silver core and $\lambda = 397$ nm.

requirements for spasing are found if one takes $w_0 = 1$, implying that all molecules are in the excited state. Then the generation can occur if $\kappa|\lambda_2''|/\gamma_\perp > 1$ [see Eq. (70)]. However, for the experimental conditions realized in Ref. [9] ($b/a \approx 3.14$), $|\lambda_2''| < 0.8$ and $\kappa|\lambda_2''|/\gamma_\perp < 2.3 \times 10^{-2}$, which is far below the threshold.

Figures 3 and 4 show the time evolution of the local-field intensity in the shell calculated using Eq. (55). This quantity can be measured, for example, in surface-enhanced Raman scattering of molecules adsorbed on the shell surface [42]. The character of this evolution depends on the ratio $\kappa/\gamma_\perp$. For a gold core this dependence is slight, which reflects the small magnitude of $\kappa|\lambda_j''|$ in comparison with $\gamma_\perp$. However, for a silver core the evolution is distinct for each value of $\kappa/\gamma_\perp$, which is explained by larger values of $|\lambda_2''|$ (see Fig. 2) and a larger contribution of the quantity $\kappa|\lambda_2''|$ to the relaxation rate. In particular, for $\kappa/\gamma_\perp = 10$ the decay curve clearly demonstrates a rapid drop which originates from plasmonic superradiance.

B. Design II

The cooperative effects in design II are determined by the quantity $\mathcal{M}$, Eq. (80). Its imaginary part, which dictates the threshold condition for spasing, is plotted in Fig. 5 for both Au and Ag shells. A comparison of Figs. 2 and 5 reveals that the threshold does not differ significantly for the two designs; however, in the latter case its dependence on the ratio a/b is more pronounced.

VII. CONCLUSION

In this paper, we have developed a first-principles theory of cooperative optical effects in a core-shell nanoparticle. We have considered two designs of such a structure in which the core (shell) is metallic and the shell (core) is doped with a large number of two-level quantum emitters. We assumed that the transition frequency of the emitters is close to the dipole surface plasmon frequency of the metallic core (shell). Taking advantage of the small size of the nanoparticle in comparison with the wavelength of the emitted radiation, we have reduced the problem under consideration to a quasistatic one.

We have described the polarization of a large number of emitters by a continuous distribution of polarization (polarium) and derived an integral equation for it. Being an integral

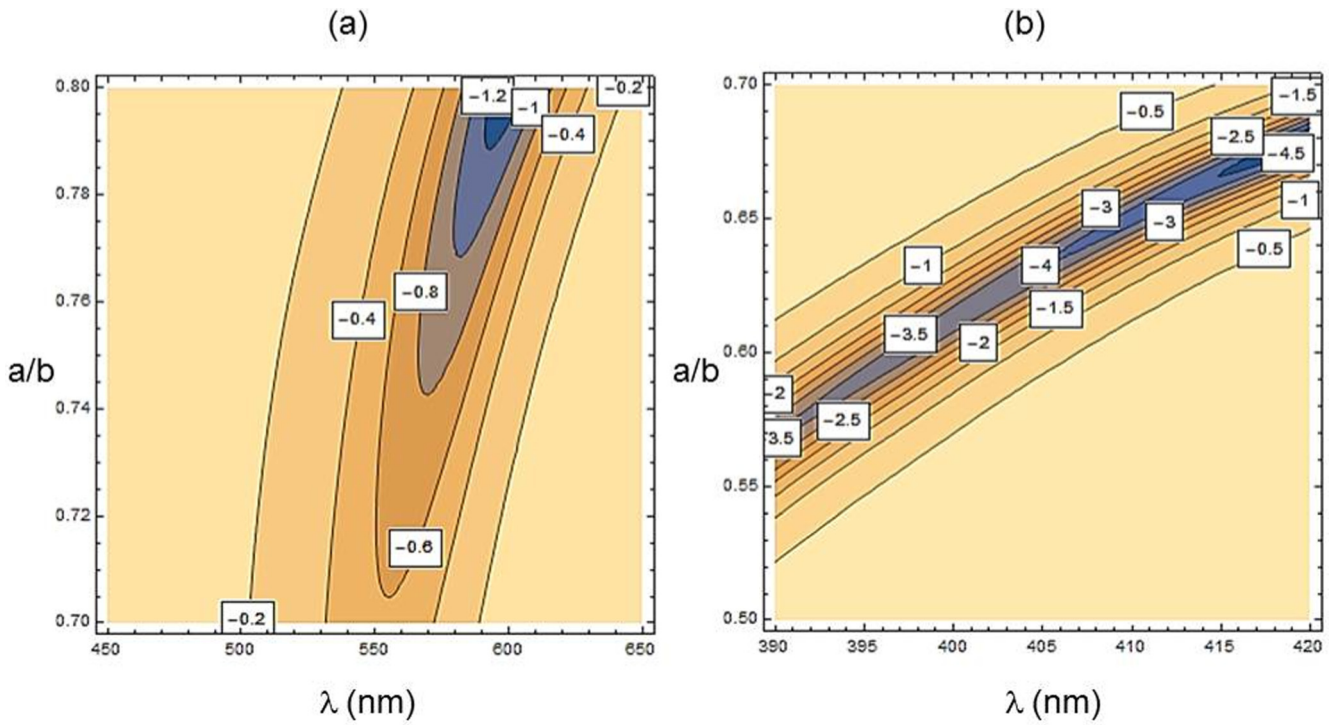

FIG. 5. Contour plots of $\mathrm{Im}\mathcal{M}$ in the vicinity of the resonance between the molecule transition ($\lambda = 2\pi c/\omega_0$) and the dipole plasmon mode ($l = 1$). (a) Gold shell. (b) Silver shell.

equation with a degenerate kernel, it is reduced to a set of two algebraic equations which has been solved analytically.

We have shown that the plasmonic superradiance and spasing are intimately related to each other. Not depending on the specific optical process under consideration, the field evolution is determined by the eigenvalues of the matrix $\hat{M}$, Eqs. (38)–(41), for design I and by the quantity $\mathcal{M}$, Eq. (80), for design II. These quantities are determined by the ratio of the two radii of the core-shell nanoparticle rather than by their absolute values, which suggests a scaling law for similar nanoparticles.

The analytical theory gives also simple and physically transparent criteria for the significance of the plasmonic Dicke effect and for the spasing threshold condition. In particular, we have shown that surface plasmon generation in a single nanoparticle for the parameters used in the experiment (Ref. [9]) is impossible. The theory reveals that spasing in the system is possible only if the plasmonic superradiance in such a system prevails over the phase relaxation. Such a situation is displayed as a rapid drop in the local-field-intensity evolution (see Fig. 4), which can be observed in surface-enhanced Raman scattering.

Although the discussion in this paper is limited to the plasmonic Dicke effect and spaser generation, the other optical processes in core-shell nanoparticles can be investigated on the same grounds. For example, surface-enhanced Raman scattering at Raman active molecules adsorbed on the nanoparticle surface can be described by assuming that there is an external electromagnetic field oscillating at the frequency close to the transition frequency in quantum emitters.

APPENDIX A: COEFFICIENTS α_{1l}, α_{2l}, β_{1l}, β_{2l}, AND δ_l

The coefficients α_{1l}, α_{2l}, β_{1l}, and β_{2l} are found from the set of four algebraic equations which follow from the boundary conditions. They can be represented in a compact form as follows:

$$\begin{aligned}
\alpha_{1l}(\omega) &= \beta_{2l}(\omega) = \frac{1}{(2l+1)\epsilon_2}\alpha_l(\omega)\beta_l\gamma_l(\omega),\\
\alpha_{2l}(\omega) &= -\frac{1}{(2l+1)\epsilon_2}\beta_l\gamma_l(\omega),\\
\beta_{1l}(\omega) &= -\frac{1}{(2l+1)\epsilon_2}\alpha_l(\omega)\gamma_l(\omega),
\end{aligned} \tag{A1}$$

where

$$\alpha_l(\omega) = \frac{l[\epsilon_1(\omega)-\epsilon_2]a^{2l+1}}{l\epsilon_1(\omega)+(l+1)\epsilon_2} \tag{A2}$$

is the l-pole polarizability of a spherical nanoparticle embedded in an infinite medium with the dielectric function ϵ_2,

$$\beta_l = \frac{l+1}{b^{2l+1}}\frac{\epsilon_3-\epsilon_2}{l\epsilon_2+(l+1)\epsilon_3}, \tag{A3}$$

and

$$\gamma_l(\omega) = \frac{1}{1-\alpha_l(\omega)\beta_l}. \tag{A4}$$

The coefficient δ_l which enters Eq. (74) is defined as follows:

$$\begin{aligned}
\delta_l(\omega) = &\frac{l+1}{l(2l+1)\epsilon_1}\frac{\alpha_l(\omega)\gamma_l(\omega)}{a^{2(2l+1)}}\\
&\times\left[1-\frac{l}{l+1}\frac{(l+1)\epsilon_1+l\epsilon_2(\omega)}{\epsilon_1-\epsilon_2(\omega)}\beta_l(\omega)a^{2l+1}\right].
\end{aligned} \tag{A5}$$

APPENDIX B: MATRIX ELEMENTS M_{ij}

The matrix elements M_{ij} are found as follows:

$$M_{11} = \alpha_{11}N_{12} + \alpha_{21}N_{11}, \tag{B1}$$

$$M_{12} = \alpha_{11}N_{22} + \alpha_{21}N_{21}, \tag{B2}$$

$$M_{21} = \beta_{11}N_{12} + \beta_{21}N_{11}, \tag{B3}$$

$$M_{22} = \beta_{11}N_{22} + \beta_{21}N_{21}, \tag{B4}$$

where

$$N_{11} \equiv \int_V |\mathbf{f}_{10}(\mathbf{x})|^2 d\mathbf{x}, \tag{B5}$$

$$N_{12} \equiv \int_V \mathbf{f}_{10}(\mathbf{x})\cdot\mathbf{g}^*_{10}(\mathbf{x})d\mathbf{x}, \tag{B6}$$

$$N_{21} \equiv \int_V \mathbf{g}_{10}(\mathbf{x})\cdot\mathbf{f}^*_{10}(\mathbf{x})d\mathbf{x}, \tag{B7}$$

$$N_{22} \equiv \int_V |\mathbf{g}_{10}(\mathbf{x})|^2 d\mathbf{x}. \tag{B8}$$

To calculate the matrix elements N_{ij} we use the representation of the nabla operator in the spherical coordinates. Namely, for two arbitrary axially symmetric functions $p(r,\theta)$ and $q(r,\theta)$, one has

$$\nabla p\cdot\nabla q = \frac{\partial p}{\partial r}\frac{\partial q}{\partial r} + \frac{1}{r^2}\frac{\partial p}{\partial\theta}\frac{\partial q}{\partial\theta}, \tag{B9}$$

whereas the volume element is given by

$$d\mathbf{x} = r^2\sin\theta dr d\theta d\varphi. \tag{B10}$$

Then, taking into account that $Y_{10}(\theta) = \sqrt{3/4\pi}\cos\theta$, one obtains

$$\begin{aligned}
N_{11} &= \int_V \nabla[rY_{10}(\theta)]\cdot\nabla[rY^*_{10}(\theta)]d\mathbf{x}\\
&= \int_0^{2\pi}\int_0^{\pi}\int_a^b\left[Y^2_{10}(\theta)+\left(\frac{\partial Y_{10}(\theta)}{\partial\theta}\right)^2\right]r^2\sin\theta dr d\theta d\varphi\\
&= b^3-a^3,
\end{aligned} \tag{B11}$$

$$\begin{aligned}
N_{22} &= \int_V \nabla\left[\frac{Y_{10}(\theta)}{r^2}\right]\cdot\nabla\left[\frac{Y^*_{10}(\theta)}{r^2}\right]d\mathbf{x}\\
&= \int_0^{2\pi}\int_0^{\pi}\int_a^b\left[\left(\frac{2}{r^3}\right)^2 Y^2_{10}(\theta)\right.\\
&\quad\left.+\frac{1}{r^6}\left(\frac{\partial Y_{10}(\theta)}{\partial\theta}\right)^2\right]r^2\sin\theta dr d\theta d\varphi = 2\left(\frac{1}{a^3}-\frac{1}{b^3}\right),
\end{aligned} \tag{B12}$$

$$N_{12} = N_{21}^{*} = \int_V \nabla[rY_{10}(\theta)] \cdot \nabla\left[\frac{Y_{10}^{*}(\theta)}{r^2}\right] d\mathbf{x}$$
$$= \int_0^{2\pi}\int_0^{\pi}\int_a^b \left[-\frac{2}{r^3}Y_{10}^2(\theta) + \frac{1}{r^3}\left(\frac{\partial Y_{10}(\theta)}{\partial\theta}\right)^2\right] r^2 \sin\theta dr d\theta d\varphi = 0. \quad \text{(B13)}$$

Finally, one finds

$$M_{11} = \alpha_{21}(b^3 - a^3), \quad \text{(B14)}$$
$$M_{12} = 2\alpha_{11}\left(\frac{1}{a^3} - \frac{1}{b^3}\right), \quad \text{(B15)}$$
$$M_{21} = \beta_{21}(b^3 - a^3), \quad \text{(B16)}$$
$$M_{22} = 2\beta_{11}\left(\frac{1}{a^3} - \frac{1}{b^3}\right). \quad \text{(B17)}$$

[1] T. W. Ebbesen, C. Genet, and S. I. Bozhevolnyi, Phys. Today, **61**(5), 44 (2008).
[2] W. L. Barnes, A. Dereux, and T. W. Ebbesen, Nature (London) **424**, 824 (2003).
[3] A. V. Kabashin, P. Evans, S. Pastkovsky, W. Hendren, G. A. Wurtz, R. Atkinson, R. Pollard, V. A. Podolskiy, and A. V. Zayats, Nat. Mater. **8**, 867 (2009).
[4] A. Hartschuh, E. J. Sánchez, X. S. Xie, and L. Novotny, Phys. Rev. Lett. **90**, 095503 (2003).
[5] J. A. Schuller, E. S. Barnard, W. Cai, Y. C. Jun, J. S. White, and M. L. Brongersma, Nat. Mater. **9**, 193 (2010).
[6] D. J. Bergman and M. I. Stockman, Phys. Rev. Lett. **90**, 027402 (2003).
[7] M. I. Stockman, J. Opt. **12**, 024004 (2010).
[8] R.-M. Ma, R. F. Oulton, V. J. Sorger, and X. Zhang, Laser Photon. Rev. **7**, 1 (2013).
[9] M. A. Noginov, G. Zhu, A. M. Belgrave, R. Bakker, V. M. Shalaev, E. E. Narimanov, S. Stout, E. Herz, T. Suteewong, and U. Wiesner, Nature (London) **460**, 1110 (2009).
[10] X. F. Li and S. F. Yu, Opt. Lett. **35**, 2535 (2010).
[11] A. De Luca, M. Ferrie, S. Ravaine, M. La Deda, M. Infusino, A. R. Rashed, A. Veltri, A. Aradian, N. Scaramuzza, and G. Strangi, J. Mater. Chem. **22**, 8846 (2012).
[12] N. Calander, D. Jin, and E. M. Goldys, J. Phys. Chem. C **116**, 7546 (2012).
[13] A. Veltri and A. Aradian, Phys. Rev. B **85**, 115429 (2012).
[14] H. Zhang, J. Zhou, W. Zou, and M. He, J. Appl. Phys. **112**, 074309 (2012).
[15] X.-L. Zhong and Z.-Y. Li, Phys. Rev. B **88**, 085101 (2013).
[16] Y. Huang, X. Bian, Y. X. Ni, A. E. Miroshnichenko, and L. Gao, Phys. Rev. A **89**, 053824 (2014).
[17] Y. Huang, J. J. Xiao, and L. Gao, Opt. Express **23**, 8818 (2015).
[18] N. Arnold, K. Piglmayer, A. Kildishev, and T. A. Klar, Opt. Mater. Express **5**, 2546 (2015).
[19] N. Arnold, C. Hrelescu, and T. A. Klar, Ann. Phys. (Berlin, Ger.) **528**, 295 (2016).
[20] M. C. Gather, Nat. Photon. **6**, 708 (2012).
[21] V. G. Bordo, Phys. Rev. A **88**, 013803 (2013).
[22] E. M. Purcell, Phys. Rev. **69**, 681 (1946).
[23] V. N. Pustovit, A. M. Urbas, A. V. Chipouline, and T. V. Shahbazyan, Phys. Rev. B **93**, 165432 (2016).
[24] J. Cuerda, F. J. García-Vidal, and J. Bravo-Abad, ACS Photon. **3**, 1952 (2016).
[25] V. M. Parfenyev and S. S. Vergeles, Opt. Express **22**, 13671 (2014).
[26] M. Richter, M. Gegg, T. S. Theuerholz, and A. Knorr, Phys. Rev. B **91**, 035306 (2015).
[27] Y. Zhang and V. May, J. Chem. Phys. **142**, 224702 (2015).
[28] R. Dicke, Phys. Rev. **93**, 99 (1954).
[29] A. V. Andreev, V. I. Emel'yanov, and Yu. A. Il'inskii, Sov. Phys. Usp. **23**, 493 (1980).
[30] S. Prasad and R. J. Glauber, Phys. Rev. A **61**, 063814 (2000).
[31] S. Prasad and R. J. Glauber, Phys. Rev. A **82**, 063805 (2010).
[32] V. N. Pustovit and T. V. Shahbazyan, Phys. Rev. Lett. **102**, 077401 (2009).
[33] V. N. Pustovit and T. V. Shahbazyan, Phys. Rev. B **82**, 075429 (2010).
[34] I. E. Protsenko and A. V. Uskov, Quantum Electron. **45**, 561 (2015).
[35] J. A. Gordon and R. W. Ziolkowski, Opt. Express **15**, 2622 (2007).
[36] J. D. Jackson, *Classical Electrodynamics* (Wiley, New York, 1998).
[37] M. Born and E. Wolf, *Principles of Optics* (Pergamon, Oxford, 1970).
[38] H. Haken, *Light* (North-Holland, Amsterdam, 1985), Vol. 2.
[39] A. D. Polyanin and A. V. Manzhirov, *Handbook of Integral Equations* (CRC Press, Boca Raton, FL, 2008).
[40] R. H. Pantell and H. E. Puthoff, *Fundamentals of Quantum Electronics* (Wiley, New York, 1969).
[41] M. Scheibner, T. Schmidt, L. Worschech, A. Forchel, G. Bacher, T. Passow, and D. Hommel, Nat. Phys. **3**, 106 (2007).
[42] G. M. Herrera, A. C. Padilla, and S. P. Hernandez-Rivera, Nanomaterials **3**, 158 (2013).